International Journal of Engineering Trends and Technology
ISSN: 2231–5381 / https://doi.org/10.14445/22315381/IJETT-V73I9P102

Volume 73 Issue 9, 10-19, September 2025

Original Article

A Dual-Band Conformal Implantable Monopole Antenna for the 915 MHz and 2.45 GHz ISM Bands

Rula Alrawashdeh

Department of Electrical Engineering, Mutah University, Alkarak, Jordan.

Corresponding Author : rular18@mutah.edu.jo

Received: 21 April 2025 Revised: 26 August 2025 Accepted: 03 September 2025 Published: 30 September 2025

Abstract - *This paper presents a monopole antenna for implantable applications in the 902-928 MHz and 2.4-2.5 GHz Industrial Scientific and Medical (ISM) bands. The antenna has a planar structure conformal to rectangular implants with overall dimensions of 20×20×0.4 mm3. It obtains a maximum gain of -20.9 and -29 dBi and a radiation efficiency of 0.43 and 0.15% at 915 MHz and 2.45 GHz, respectively. It also has obtained a bandwidth of 32 and 20% around the above-mentioned frequencies, which is wide enough to maintain good matching below -10 dB in the real human body. The proposed antenna has obtained a relatively large gain value at 915 MHz in comparison with other conformal or flexible antennas proposed in the literature. It is probably the smallest antenna proposed in literature with the largest gain, wider bandwidth and dual band functionality at 915 MHz and 2.45 GHz ISM bands.*

Keywords - *Conformal antennas, 915 MHz, Implantable antennas, ISM.*

1. Introduction

Bio-telemetric healthcare applications are mainly facilitated by wireless communication in which data are transmitted by implantable antennas placed inside the human body [1]. To facilitate long and stable communication, the implantable antenna should satisfy a set of requirements, including a small size to fit inside small implantable devices. It is also required to be biocompatible and light in weight, which requires specific materials. Moreover, while high frequencies are preferred for high data rates, they cause larger attenuations for the signals inside the human body tissues, which have variant conductivity values that increase with frequency [2]. The Specific Absorption Rate (SAR) is another parameter that the implantable antenna needs to satisfy. A SAR level smaller than 1.6 W/Kg is needed for safe radiation towards the human body tissues [3]. The coverage of multiple frequency bands is another feature that is highly appealing. Some bands are required to support data transmission, while others are required to support other functionalities such as power saving and wireless power transfer [4].

Various configurations of implantable antennas have already been suggested in the literature. In [5, 6], a number of designs were proposed for the 401-406 MHz. This band represents a good choice for implantable applications, as stated above, due to the small human body attenuations at its frequency range. However, data rates are usually low in this frequency band. Also, the power efficiency is relatively small due to the small electrical size in this band. Other designs have also been proposed in [7, 8] at 2.45 GHz. While this band supports higher data rates than those at the 401-406 MHz Medical Device Radio-Communication (MedRadio) band, the human body attenuations are large at this frequency band. To overcome these limitations and to provide a compromise between the two options, designs in the 902-928 MHz band have been proposed. This frequency band provides a good choice to support higher data rates and radiation efficiency while keeping relatively small attenuations at the same time [9]. The design in [10] obtained circular polarization with a maximum gain of -29 dBi at 915 MHz via a meandered patch structure. A bear-shaped antenna was also proposed in [11] for implantable applications in the 915 MHz ISM band. That antenna was small and obtained a gain value of -28 dBi. However, it was rigid and covered one frequency band only.

Another rigid antenna of good gain and bandwidth was proposed in [12]. The antenna referenced in [13] was a coplanar waveguide-fed design, partially cut and printed on a 24 µm thick flexible substrate. To adjust the bandwidth, a 0.25 mm thick magneto-dielectric sheet is affixed to its bottom layer. This antenna reached a peak gain of −30.32 dBi. While the antenna in [14] obtained a maximum gain of -16 dBi at 910 MHz, its bandwidth was very narrow and did not cover the entire frequency range between 902 and 928 MHz. Overall, most of these 902-928 MHz designs were either rigid, narrow in bandwidth or of relatively small gain values. Monopoles are one of the desirable structures for implantable applications due to their small size. They can also be easily designed to provide

conformity. A CPW-fed monopole antenna of Z shape and H-slot were proposed in [15, 16], respectively. A spiral monopole was also proposed in [17]. However, they all worked for the 2.45 GHz ISM band. The spiral monopole in [18] was proposed for the 401.3 MHz with a very narrow bandwidth. A wider bandwidth was obtained in [19] over the same frequency range. A few monopoles were proposed for the 915 MHz band. Hence, the work was aimed at designing a monopole antenna for this frequency band. Based on the shortcomings of previous implantable antenna designs, which were mainly rigidity and single-band coverage, this work presents a conformal antenna for dual bandwidth, which are the 915 MHz and 2.45 GHz ISM bands. These frequency bands provide a good compromise between relatively high data rates and moderate attenuation levels. This antenna obtains good radiation characteristics with a maximum gain value of -20.9 dBi while obtaining a wide bandwidth at the same time. It has a small thickness of 0.4 mm, which makes it suitable to fit inside the small implantable device. Moreover, this antenna works at the 2.45 GHz ISM band, offering a dual-band functionality for power saving purposes [20].

This paper is organized into four sections: First, the antenna structure and design are presented. Then, the antenna performance is analysed, and the effect of the structural parameters is investigated. The final section provides the conclusions.

2. Design

2.1. Methodology and Methods

To obtain the design target and objectives, the design process is conducted via different steps, which can be summarized as follows:

Select the optimum antenna structure for the intended targets. This step includes investigating the optimum shape that: obtains miniaturization, has loops or spirals within to enrich the near magnetic field and decreases electrical losses inside the human body [21]. A monopole structure is selected which provides resonance over a small size in comparison with a loop or a dipole. Moreover, spirals can be easily integrated into the main radiator. Further details on the structure are provided in the following section. All these characteristics were accurately selected and optimized to overcome the limitations of existing designs.

Optimize the antenna performance (reflection coefficient and gain mainly) for the 915 MHz ISM band. This step comprises a parametric study, mainly selecting the optimum dimensions of the radiating parts and ground.

Optimize the antenna performance for the 2.45 GHz ISM band. The same evaluation parameters are targeted at this step. The optimization process during this step is conducted carefully to maintain the good performance attained for the 915 MHz ISM band.

The optimization process for the 915 and 2450 MHz bands was executed inside a simplified body model of an elliptic shape and overall dimensions of 100×100×50 mm^3. The shape and dimensions are selected to guarantee a good resemblance to the human body organs. The antenna is placed at the centre and is fully surrounded by muscle to represent deeply implanted devices.

Evaluate and analyse the antenna performance. This step includes assessing the specific absorption rate, radiation pattern and characteristics. The distances of communication are also calculated at this stage.

Validate the design using real components and materials. The antenna is fabricated at this stage, and its performance inside a pork phantom is measured. The measurement results are analysed and compared with the corresponding simulation results at this stage.

Computer Simulation Technology (CST) [22] is used for design and analysis in this work.

2.2. Materials and Structures

The antenna structure is shown in Figure 1.

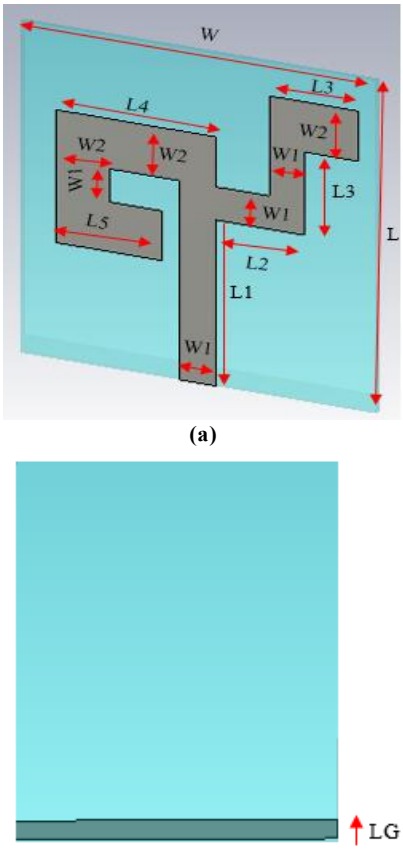

(a)

(b)

Fig. 1 The proposed structure: (a) Front view, and (b) Back view: W1= 2, W2= 3, W= 20, L1= 10, L2= 4.9, L3= 5, L4= 9, L5= 6, L= 20, LG= 1; dimensions in mm.

The antenna has a monopole structure with a quasi-rectangular ring at its left side. Monopoles have a number of appealing features for implantable applications, such as their small size (quarter wavelength) and omnidirectional radiation pattern. It also has a good gain, which is larger than that of the corresponding dipole [23]. The quasi-rectangular ring attached to the rectangular feedline was optimized in the first design step to obtain resonance at around 850 MHz and to cover the entire 902-928 MHz. The integrated loop helps to miniaturize the antenna while strengthening the near magnetic field. This may boost the antenna gain and reduce the SAR level [4, 24]. The right half of the top of the antenna, which includes a stair-step section connected to the left part of the antenna, was introduced in the second design step to increase the antenna gain by around 2.5 dBi. The ground is positioned on the antenna's backside and is only 1 mm high. The substrate has a small thickness of 0.4 mm and is made of Flame Retardant 4 (FR-4) material. This material is affordable with a relatively low loss tangent (ε_r= 4.3, tanδ= 0.025 [22]). The ground and radiator are modelled as copper, which has a good conductivity value. It is worth indicating that the antenna parameters are carefully selected to obtain a wide -10 bandwidth covering the 902-928 MHz ISM band with good margins below and above this frequency band. The maximum antenna dimensions are 20×20×0.4 mm^3. It is supposed to be a part of a rectangular implant of 20×20×10 mm^3 in size. The implant's material has a relative permittivity of 4.3. The overall structure of the implant and the antenna inside it is shown in Figure 2.

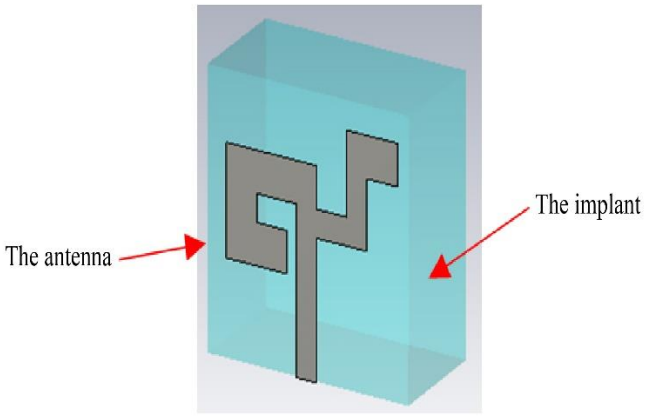

Fig. 2 The antenna inside the implant at its edge

3. Results and Performance

3.1. The Reflection Coefficient and Radiation Characteristics

The proposed antenna is aimed at implantable applications. Hence, it should perform well inside the human body. Thus, it is simulated inside a human body model of an elliptic shape and 100 mm height. It has an equivalent material of muscle at 915 MHz with the following dielectric properties (σ= 0.95 S/m and εr=55 [25]). The antenna is located in the middle of this model, as shown in Figure 3.

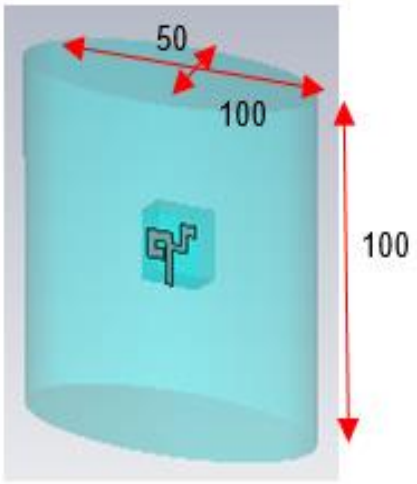

Fig. 3 The body of optimization; dimensions in mm.

The antenna has obtained a wide -10 dB bandwidth ranging between f_L=740 MHz to f_h=1.0219 GHz as plotted in Figure 4, which corresponds to a rational bandwidth ($BW_{rational}$) of 0.32:

$$BW_{rational} = 2 \times \left(\frac{f_h - f_L}{f_h + f_L}\right) \quad (1)$$

Where f_L (Hz) has the lowest band frequency and fh (Hz) has the highest band frequency.

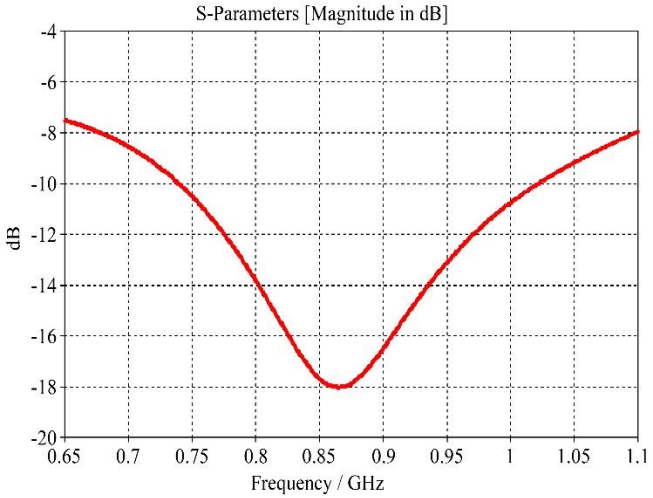

Fig. 4 The reflection coefficient S1,1 (dB) in the simplified human body model

The antenna has also obtained a radiation efficiency of 0.43% and a maximum 3D gain of -20.9 dBi. It has also obtained an omnidirectional radiation pattern, as shown in Figure 5, which is preferred for implantable applications.

It is worth noting that negative gain values are expected in this case. This is mainly due to the attenuation losses caused by the human body tissues surrounding the antenna.

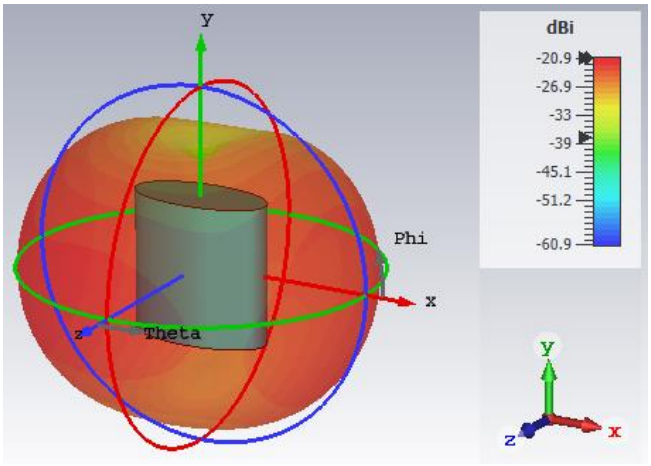

Fig. 5 The 3D gain radiation pattern at 915 MHz

For safety considerations, the simulated maximum 1-g SAR ($Max_{1\text{-}g}SAR$) is 183.942 W/kg. Based on this value, the antenna can be provided with an input power (P_{in}) of up to 8.7 mW (9.4 dBm) approximately while still satisfying the SAR limitations.

$$P_{in} = \frac{1.6}{Max_{1-g}SAR} \quad (2)$$

3.2. Parametric Study

In this section, the effect of the ground height and substrate thickness on the overall antenna performance has been investigated and studied. For the substrate, three thicknesses are attempted (hs=0.6, hs=0.8 and hs=1) in addition to the 0.4 mm thickness which has been selected as an optimum design value. The -10 dB reflection coefficient results which are shown in Figure 6 indicate that the resonant frequency shifts up with the thickness. This is because the effective permittivity decreases around the antenna (smaller area of the surrounding human body tissues).

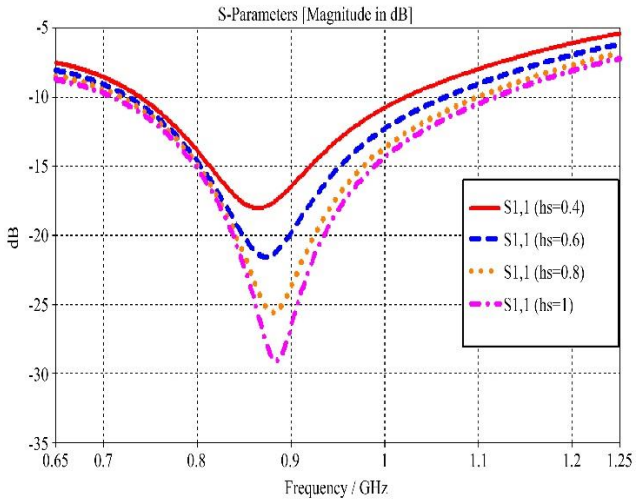

Fig. 6 The reflection coefficient S1,1 (dB) for different substrate hicknesses

However, the antenna has obtained good matching for all the simulated thicknesses. Although the bandwidth has widened for larger thicknesses, the overall size has also increased. The same antenna radiation efficiency has been almost obtained for all the substrate thicknesses. This means that the proposed antenna can be used safely with real implantable chips that are usually provided with an input power of 0 dBm [26, 27].

The ground height effect has also been investigated. The parameter yG represents the maximum height of the ground. The lower edge of the ground is located at -10. Hence, a value of yG= -9 represents a ground height of (-9-(-10)) =1 mm). while yG = -6, -3 and 0 represent a ground height of 4, 7 and 10 mm, respectively. The -10 dB S11 is shown in Figure 7. The -10 dB bandwidth tends to narrow with increased ground height. The -10 matching level also tends to disrupt with an increased ground height. It is obvious from the figure that the deepest matching level and widest -10 dB bandwidth are obtained for a ground height of 1 mm (yG-9).

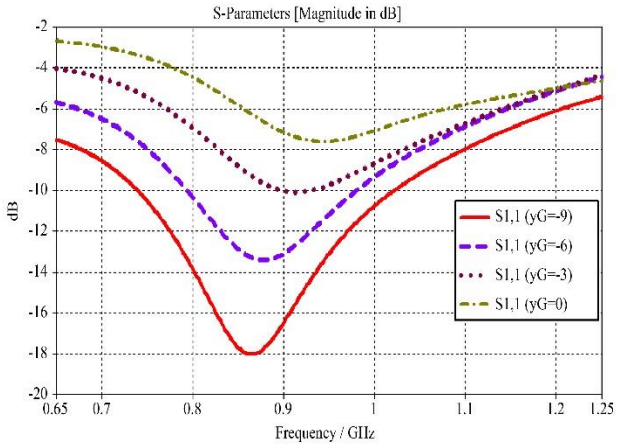

Fig. 7 The effect of the ground height on the reflection coefficient S1,1 (dB)

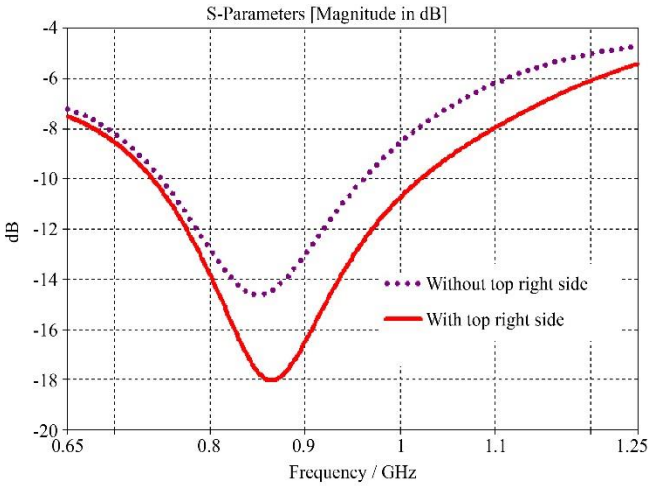

Fig. 8 The effect of the top right side of the antenna on the reflection coefficient S1,1 (dB)

In addition to the two above-mentioned parameters, the effect of the top right side of the antenna is explained in this section. The S11 results are shown in Figure 8. The figure clearly shows that adding the top right section significantly widens the antenna's -10 dB bandwidth. This modification also doubles the antenna's radiation efficiency and increases the gain by 2.5 dBi. These improvements are primarily due to the introduction of additional radiating elements.

3.3. Performance in the 2.45 GHz ISM Band

The antenna is optimized to work at the 2.45 GHz ISM band, which can be exploited for wireless power transfer or energy harvesting for the implantable device [5]. This enables charging the battery wirelessly or powering the device directly without the need for surgeries for battery replacement or charging [28]. This is obtained by adding a section that is longer than ($\lambda ib/4 = \lambda 0/4\sqrt{\varepsilon r}$) at 3 mm from the feedline edge while keeping all the dimensions of the original antenna the same. The modified antenna structure is shown in Figure 9.

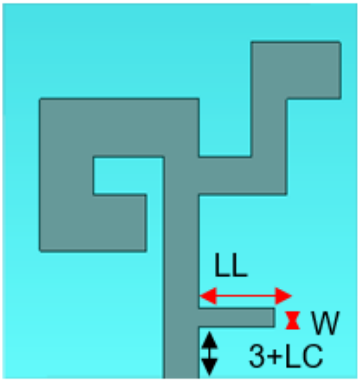

Fig. 9 The modified antenna structure for performance in the 2.45 GHz ISM band (LL=4, W=1, LC=0); dimensions in mm

The antenna is simulated in the simplified body model of the same structure and dimensions, but with the following dielectric properties (σ= 0.95 S/m and ε_r=55 [25]).

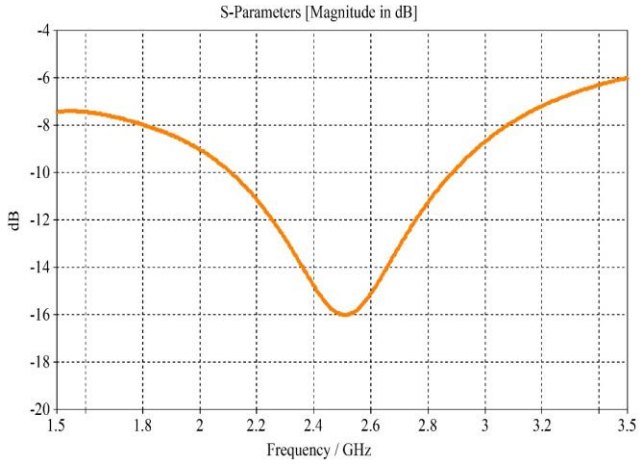

Fig. 10 The reflection coefficient S1,1 (dB) of the modified antenna for the 2.4-2.5 GHz ISM band

It obtains a deep matching below S11=-10 dB over the entire 2.4 to 2.5 GHz ISM frequency band, as shown in Figure 10. The effect of the added section parameters on the antenna performance in this frequency band is investigated in this section. First, the effect of the section length (LL), which can be represented in terms of λ_{ib} (m), is studied:

$$\lambda_{ib} = \frac{\lambda_0}{\sqrt{\varepsilon_r}} = \frac{c}{f_0\sqrt{\varepsilon_r}} \quad (3)$$

Where λ_0 (m) is the free space wavelength, ε_r is the relative permittivity and c (m/s) is the velocity of propagation of electromagnetic waves in free space.

Four lengths are simulated, which are: $\lambda ib/10$= 1.6981 mm, $\lambda ib/4$= 4.25 mm, $\lambda ib/3$= 5.661 mm and $\lambda ib/2$=8.491 mm. The result of the reflection coefficient S1,1 is shown in the following Figure.

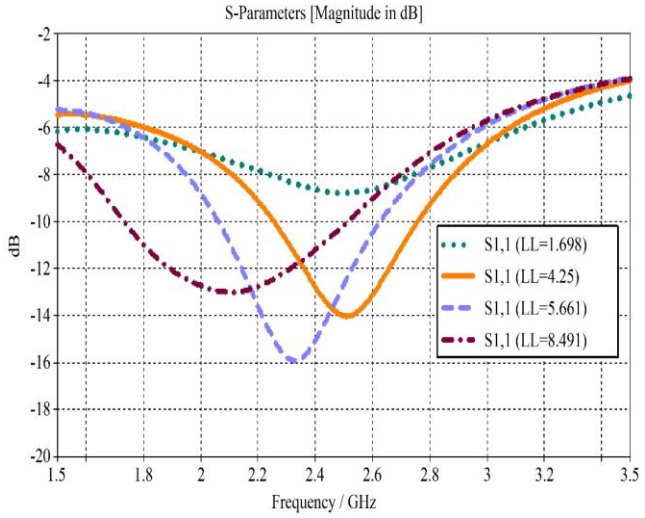

Fig. 11 The effect of the added section length on the simulated reflection coefficient S1,1 (dB)

It can be seen from the figure that the antenna obtains a good matching for a length of 4.25 and 5.66 mm, which represent ($\lambda ib/4$) and ($\lambda ib/3$), respectively. No matching is obtained when the antenna is electrically short (LL=1.6981 mm). Generally, the resonant frequency shifts down when LL increases. The effect of the section location is also studied. Four locations are examined while keeping W=1 and LL=4.25 mm. The resultant simulated reflection coefficient (S11) is shown in Figure 12. The resonance tends to shift up when this section is located at 2 mm (Lc= -1 mm) from the feedline edge, while it tends to shift down as this distance increases to 4 (Lc= 1) and 5 (Lc= 2) mm, respectively. The optimum spacing is found at Lc=0 mm, which corresponds to a spacing of 3 mm from the feedline edge. The frequency band (2.256-2.758 GHz) is centered with this spacing at around 2.45 GHz, and the overall percentage bandwidth is 20%.

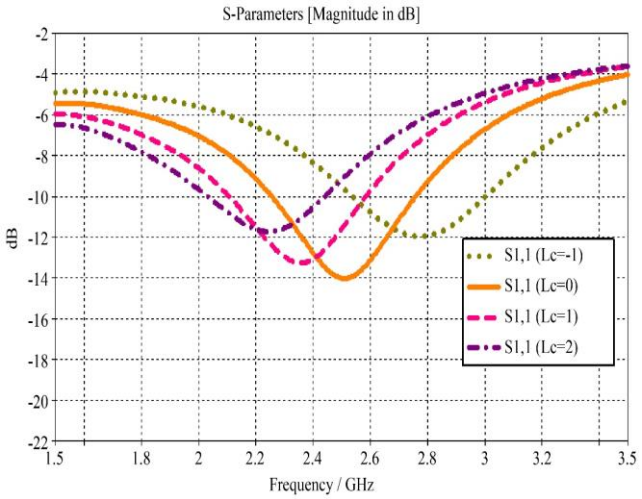

Fig. 12 The effect of the added section location on the reflection coefficient S1,1 (dB) of the proposed antenna

The third parameter of investigation is the added section width (W). The simulated reflection coefficient for three width values is shown in Figure 13.

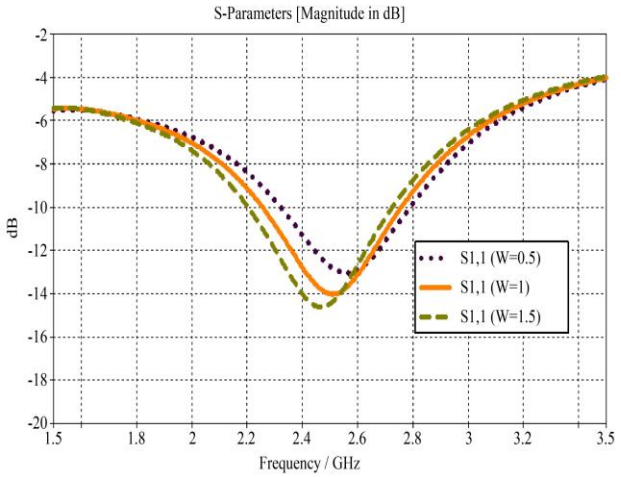

Fig. 13 The effect of the added section width on the reflection coefficient S1,1 (dB)

The results show that the resonant frequency tends to shift up for a thinner section and to shift down for a thicker section.

The thickness of 1 mm represents a good choice for the proposed design as it obtains good matching while keeping the frequency band of interest centralized with good margins below the minimum and maximum frequencies.

The total radiation efficiency and gain obtained at 2.45 GHz are -29 dBi and 0.15%, respectively. The maximum 1-g SAR is 163.4 W/kg.

The antenna obtains a maximum radiation in the azimuth plane at an angle of 25 degrees, as shown in Figure 14.

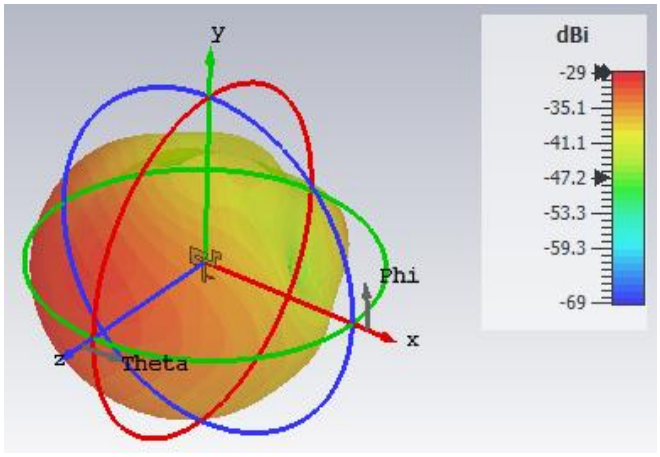

Fig. 14 The 3D gain radiation pattern at 2.45 GHz

After adding this section, it is worth pointing out that the antenna has maintained almost the same matching and resonance in the 902-928 MHz ISM band. A stronger current exists at the 2.45 GHz than at the 915 MHz around the added section, as shown in Figure 15. This is attributed to the larger electrical length of this section at 2.45 GHz than that at 915 MHz. It has an effective electrical length of a quarter in body wavelength at 2.45, while it has an electrical length of only a tenth in the body wavelength at 915 MHz.

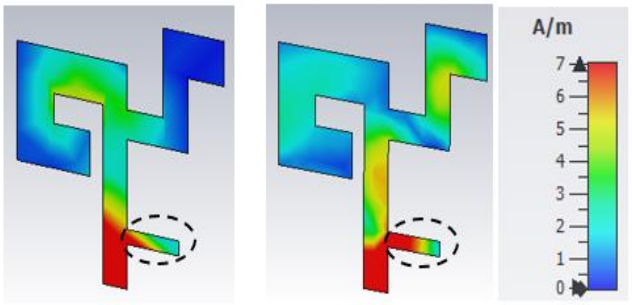

(a) **(b)**

Fig. 15 The surface current (A/m) at: (a) 915 MHz, and (b) 2.45 GHz.

4. Validation

The antenna is fabricated as shown in Figure 16 and measured to validate its performance. The main radiator is realized by using a flexible copper tape, while the substrate is made of a paper material.

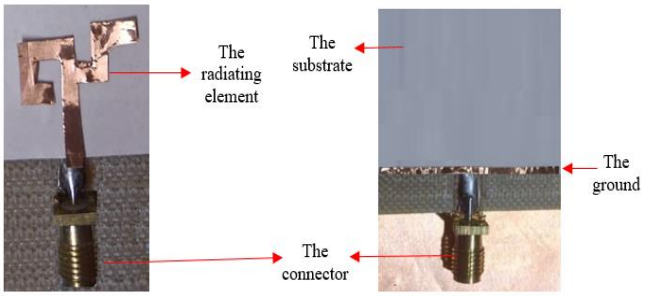

Fig. 16 The fabricated antenna: (a) Front view, and (b) Back view.

Measurements are conducted for the antenna wrapped inside pork with dielectric properties similar to the human body [19]. The measurement setup is shown in Figure 17.

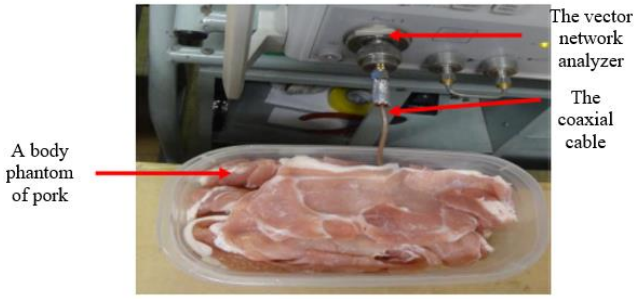

Fig.17. The measurement setup

The antenna is wrapped by an isolating layer in order to avoid direct contact between the antenna and the feeding coaxial cable from the surrounding lossy pork material. The results of the measured The results are shown in Figure 18. A slightly wider bandwidth is obtained for measurements in comparison with simulations. However, the results clearly indicate that deep matching (S1,1 <-10 dB) is always obtained and maintained for both bands as desired.

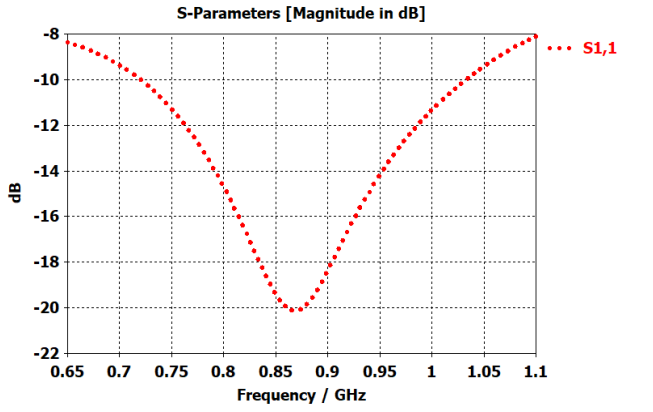

(a)

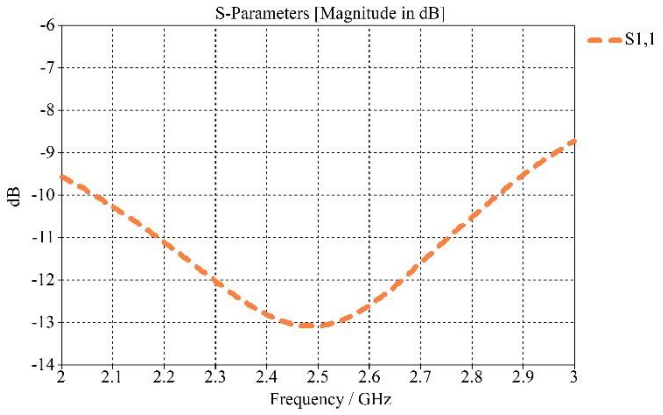

(b)

Fig. 18 The measurement results for the: (a) 915 MHz, and (b) 2.45 GHz ISM bands.

5. Link Budget Calculations

In this section, the capability of the antenna to radiate signals from the human body to external receivers in the farfield is evaluated. A communication path link of the parameters summarized in Table 1 is assumed.

Table 1. Parameters of a communication path link

Parameter	Symbol	Unit	Value
Frequency	f	MHz	915
			2450
Transmitting antenna gain	G_{tx}	dBi	-20.9
			-29
Receiving antenna gain	G_{rx}		2.15
			5.19
Transmitted power	P_{tx}	dBm	0
Receiver sensitivity	P_{rx}		-99 at 915 MHz
			-85 at 2450 MHz
Cable loss	L_c	dB	0.5
Path loss exponent	n	-----	3
Link margin	LM	dB	3

The distance over which the antenna can communicate can be calculated as follows:

$$P_{rx} = P_{tx} + G_{tx} + G_{rx} - 10n\log_{10}\left(\frac{4\pi d}{\lambda}\right) - L_c - LM \quad (4)$$

The value of the input power is common for implantable devices. It is also smaller than the limits allowed based on the SAR results. Two different values for the receiver sensitivity are assumed, with a smaller one at 2.45 GHz. Two values are considered for the receiver antenna gain, which can be simply achieved with typical half-wave dipole or monopole antennas, given that the receiver antenna size is less restricted than the implantable one. The 2.15 dBi gain is small enough to consider a worst-case scenario. A link margin of 3 dB is assumed to consider extra losses that may arise during the communication process inside the complicated human body environment. Considering all of the above parameters, the calculated distances at both bands are summarized in Table 2.

Table 2. Calculated distance of communication

Frequency f (MHz)	Gain G_{rx} (dBi)	Distance D (m)
915	2.15	9.4
	5.19	11.9
2450	2.15	0.64
	5.19	0.82

The results indicate that longer communication ranges can always be obtained at 915 MHz, which is expected for the lower path loss attenuations obtained at such frequencies in comparison with those for higher frequencies. A distance of up to 11.9 m is obtained with this frequency for this case. It is

worth indicating that while shorter distances are obtained at 2.45 GHz, performance at this frequency will be mainly for receiver wake-up purposes and not for data transmission.

6. Comparison with Existing Work in Literature

The antenna is compared with other implantable antennas proposed for the 915 MHz. The comparison is summarized in Table 3. The antennas in [10, 11, 13, 30] obtained smaller gain values than the design proposed in this paper. The antenna in [12] obtained a relatively large gain value due to the small skin thickness in which the antenna is simulated and evaluated. The small gain values usually obtained for implantable antennas are mainly due to the lossy material around them, and it tends to underestimate when antennas are simulated in small lossy layers. The antenna in [29] is narrow in bandwidth. The design in [14] was also narrow in bandwidth. Although the antenna in [31] had a small size, it obtained small gain values despite its simulation inside fat, which has much smaller conductivity than muscle [25]. In addition, although the antenna in [32] worked for two frequency bandwidths, its gain at both bands was smaller than that of our antenna. This also applies to the design in [34]. Although the design in [33] was of dual bandwidth and small, it was for an on-body antenna over short distances, while the designs in [35, 36] worked for a single bandwidth only. The comparison indicates that the proposed antenna is the smallest antenna of the largest gain and wider bandwidth with dual band functionality at 915 MHz and 2.45 GHz ISM bands.

Table 3. A comparison between the proposed antenna and other existing antennas in the literature for the 915 MHz

Reference	Freq range (MHz)	Dimensions (mm)	Gain (dBi)	Rad Eff (%)
[10]	889-924	11×11× 1.27	-29	------
[11]	860-1080	7×7× 0.254	-22 at 915	2.2 at 915
[12]	~ 740-980	4×4× 0.3	3.22 at 915	------
[13]	810-1062	4×12× 0.274	-30.32 at 915	------
[14]	900-920	6×7.8× 0.635	-16 at 915	------
[29]	902-944.21	26×54× 0.2	-3.94 at 915	14.86 at 915
[30]	800-1000	7×7× 0.254	-28 at 915	2.2 at 915
[31]	328-450 900-1070 2250-2500	6×5×0.5	-47.7 at 403 -37.2 at 915 -25.5 at 2450	0.0006 at 403 0.006 at 915 0.06 at 2450
[32]	1395–1432 2400–2500	5×5×0.635	-32.1 at 1400 -31.5 at 2450	------
[33]	2400–24835 5725–5875	5× 5×1.016	------	------
[34]	241–641 1170–2060	27× 14×1.6	-48.4 at 467 –36 at 1690	------
[35]	830-1018	7 × 7 × 0.25	−26.2 dBi at 915 MHz	------
[36]	2.3–3.03	6 mm × 6 mm× 0.53	−19.92 dB	60, 60, 47
This work	740-1021.9 2256- 2758	20×20×0.4	-20.9 at 915 -29 at 2450	0.43 at 915 0.15 at 915

7. Conclusion

In this paper, a monopole antenna is optimized and developed for implantable applications in the 915 MHz and 2.45 GHz ISM bands. The antenna has obtained a wide bandwidth of 32% and a maximum 3D-gain of -20.9 dBi at 915 MHz. It also has obtained a bandwidth of 20% and a maximum gain of -29 dBi at 2.45 GHz. The antenna exploits a quasi-rectangular ring and stair-step section to optimize its radiation characteristics inside the lossy human body. It also has obtained a maximum 1-g SAR of 183.942 and 163.4 W/kg, and thus it can be provided with up to 8.7 mW (9.4 dBm) approximately while still satisfying the safety SAR limitations. The effect of the substrate thickness and ground height has been investigated, and a robust performance of the antenna has been indicated for the various parameters. The effect of adding an extra radiating part to the antenna has also been studied, indicating that adding such a part can improve the antenna gain by up to 2.5 dB and double the radiation efficiency.

Acknowledgments

This work is supported by Mutah University in Jordan.

References

[1] Md Mohiuddin Soliman et al., "Review on Medical Implantable Antenna Technology and Imminent Research Challenges," *Sensors*, vol. 21, no. 9, pp. 1-28, 2021. [CrossRef] [Google Scholar] [Publisher Link]

[2] Jian Feng Zhao et al., "A Review on Human Body Communication: Signal Propagation Model, Communication Performance, and Experimental Issues," *Wireless Communications and Mobile Computing*, vol. 2017, pp. 1-15, 2017. [CrossRef] [Google Scholar] [Publisher Link]

[3] "C95.1-2005 - IEEE Standard for Safety Levels with Respect to Human Exposure to Radio Frequency Electromagnetic Fields, 3 kHz to 300 GHz," *IEEE Std C95.1-2005 (Revision of IEEE Std C95.1-1991)*, pp. 1-238, 2006. [CrossRef] [Google Scholar] [Publisher Link]

[4] Jamal Nasir et al., "Miniaturized Quad-Band Implantable Antenna for Wireless Capsule Endoscopy and Deep Tissue Monitoring Applications," *IEEE Transactions on Antennas and Propagation*, vol. 73, no. 8, pp. 5333-5345, 2025. [CrossRef] [Google Scholar] [Publisher Link]

[5] Tarakeswar Shaw, and Debasis Mitra, "Wireless Power Transfer System Design for Biomedical Implants at 2.45 GHz," *2019 IEEE Asia-Pacific Microwave Conference (APMC)*, Singapore, pp. 717-719, 2019. [CrossRef] [Google Scholar] [Publisher Link]

[6] Jingchen Wang et al., "Design of an Implantable Antenna for Wireless Communication of Ingestible Capsule Endoscope," *2019 International Symposium on Antennas and Propagation (ISAP)*, Xi'an, China, pp. 1-3, 2019. [Google Scholar] [Publisher Link]

[7] Ahmed Z.A. Zaki et al., "Design and Modeling of Ultra-Compact Wideband Implantable Antenna for Wireless ISM Band," *Bioengineering*, vol. 10, no. 2, pp. 1-19, 2023. [CrossRef] [Google Scholar] [Publisher Link]

[8] Daibin Jing et al., "Compact and Broadband Circularly Polarized Implantable Antenna for Wireless Implantable Medical Devices," *IEEE Antennas and Wireless Propagation Letters*, vol. 22, no. 6, pp. 1236-1240, 2023. [CrossRef] [Google Scholar] [Publisher Link]

[9] Joan Gemio, Josep Parron, and J. Soler, "Human Body Effects on Implantable Antennas for ISM Bands Applications: Models Comparison and Propagation Losses Study," *Progress in Electromagnetics Research*, vol. 110, pp. 437-452, 2010. [CrossRef] [Google Scholar] [Publisher Link]

[10] Changrong Liu, Yudi Zhang, and Xueguan Liu, "Circularly Polarized Implantable Antenna for 915 MHz ISM-Band Far-Field Wireless Power Transmission," *IEEE Antennas and Wireless Propagation Letters*, vol. 17, no. 3, pp. 373-376, 2018. [CrossRef] [Google Scholar] [Publisher Link]

[11] Sarosh Ahmad et al., "A Wideband Bear-Shaped Compact Size Implantable Antenna for In-Body Communications," *Applied Sciences*, vol. 12, no. 6, pp. 1-13, 2022. [CrossRef] [Google Scholar] [Publisher Link]

[12] Nabeel Ahmed Malik et al., "A Compact Size Implantable Antenna for Bio-medical Applications," *2020 International Conference on UK-China Emerging Technologies (UCET)*, Glasgow, UK, pp. 1-4, 2020. [CrossRef] [Google Scholar] [Publisher Link]

[13] Zhihao Luan et al., "Design of an Implantable Antenna Operating at ISM Band Using Magneto-Dielectric Material," *Progress in Electromagnetics Research Letters*, vol. 82, pp. 65-72, 2019. [CrossRef] [Google Scholar] [Publisher Link]

[14] S. Ashok Kumar, and T. Shanmuganantham, "Scalp-Implantable Antenna for Biomedical Applications," *2020 URSI Regional Conference on Radio Science (URSI-RCRS)*, Varanasi, India, pp. 1-4, 2020. [CrossRef] [Google Scholar] [Publisher Link]

[15] S. Ashok Kumar, and T. Shanmuganantham, "Implantable Monopole Antennas for ISM Band Applications," *2013 IEEE Applied Electromagnetics Conference (AEMC)*, Bhubaneswar, India, pp. 1-2, 2013. [CrossRef] [Google Scholar] [Publisher Link]

[16] Srinivasan Ashok Kumar, and Thangavelu Shanmuganantham, "Implantable CPW-fed Z-Monopole Antennas at 2.45 GHz ISM Band for Biomedical Applications," *International Journal of Microwave and Wireless Technologies*, Bhubaneswar, India, vol. 7, no. 5, pp. 529-533, 2015. [CrossRef] [Google Scholar] [Publisher Link]

[17] Pujayita Saha, Debasis Mitra, and Susanta Kumar Parui, "A Circularly Polarized Implantable Monopole Antenna for Biomedical Applications," *Progress in Electromagnetic Research C*, vol. 85, pp. 167-175, 2018. [CrossRef] [Google Scholar] [Publisher Link]

[18] Jabir Aziz, and Ayat Kamel, "Design of Miniaturized Printed Spiral Monopole Antena," *Al-Rafidain Journal of Engineering Sciences*, vol. 1, no. 1, pp. 24-34, 2023. [CrossRef] [Google Scholar] [Publisher Link]

[19] Amal Bouazizi et al, "A Miniaturized Implantable Monopole Antenna Design for Kidney Cancer Detection," *World Journal of Modelling and Simulation*, vol. 16, no. 1, pp. 3-10, 2020. [Google Scholar] [Publisher Link]

[20] S. Dinesh, R. Vivek Priyan, and R. Jothichitra, "Design of Implantable Patch Antenna for Biomedical Application," *2015 International Conference on Innovations in Information, Embedded and Communication Systems (ICIIECS)*, Coimbatore, India, pp. 1-6, 2015. [CrossRef] [Google Scholar] [Publisher Link]

[21] Mehrab Ramzan et al., "An Ultra-Miniaturized High Efficiency Implanted Spiral Antenna for Leadless Cardiac Pacemakers," *IEEE Transactions on Biomedical Circuits and Systems*, vol. 17, no. 3, pp. 621-632, 2023. [CrossRef] [Google Scholar] [Publisher Link]

[22] CST Studio Suite, Electromagnetic Field Simulation Software, Simulia, 2023. [Online]. Available: http://www.CST.com

[23] Yi Huang, and Kevin Boyle, *Antennas from Theory to Practice*, 2nd ed., Wiley, 2008. [Google Scholar] [Publisher Link]

[24] Anwar Tarawneh et al., "A Triple Band Flexible Antenna based on Asymmetric Spiral Split Rings Coupled to External Loop," *Jordan Journal of Energy (JJE)*, vol. 2, no. 1, pp. 1-16, 2024. [CrossRef] [Google Scholar] [Publisher Link]

[25] Daniele Andreuccetti, Roberto Fossi, and Caterina Petrucci, An Internet resource for the calculation of the Dielectric Properties of Body Tissues in the Frequency Range 10Hz-100GHz, IFAC, 1996. [Online]. Available: http://niremf.ifac.cnr.it/tissprop/

[26] Jayant Charthad et al., "A mm-Sized Implantable Medical Device (IMD) with Ultrasonic Power Transfer and a Hybrid Bi-Directional Data Link," *IEEE Journal of Solid-State Circuits*, vol. 50, no. 8, pp. 1741-1753, 2015. [CrossRef] [Google Scholar] [Publisher Link]

[27] Archana Mohan, and Niraj Kumar, "Implantable Antennas for Biomedical Applications: A Systematic Review," *BioMedical Engineering OnLine*, vol. 23, no. 1, pp. 1-29, 2024. [CrossRef] [Google Scholar] [Publisher Link]

[28] Amjad Iqbal et al., "Wireless Power Transfer System for Deep-Implanted Biomedical Devices," *Scientific Reports*, vol. 12, no. 1, pp. 1-13, 2022. [CrossRef] [Google Scholar] [Publisher Link]

[29] Kevin A. Kam et al., "A Fully Integrable 915MHz Implantable Antenna System for Long-Range Telemetry in Rodents," *2023 IEEE MTT-S International Microwave Biomedical Conference (IMBioC)*, Leuven, Belgium, pp. 55-57, 2023. [CrossRef] [Google Scholar] [Publisher Link]

[30] Sarosh Ahmad et al., "X-Shaped Slotted Patch Biomedical Implantable Antenna for Wireless Communication Networks," *Wireless Communications and Mobile Computing*, vol. 2022, pp. 1-11, 2022. [CrossRef] [Google Scholar] [Publisher Link]

[31] Nabeel Ahmed Malik, "*Design of Implantable Antennas for Biomedical Application*," Ph.D. Dissertation, Department of Computer Science and Technology, University of Bedfordshier, 2022. [Google Scholar] [Publisher Link]

[32] Majdi Bahrouni et al., "Modeling of a Compact, Implantable, Dual-Band Antenna for Biomedical Applications," *Electronics*, vol. 12, no. 6, pp. 1-15, 2023. [CrossRef] [Google Scholar] [Publisher Link]

[33] Yara A. Kamel et al., "RF Communication between Dual Band Implantable and on Body Antennas for Biotelemetry Application," *Scientific Reports*, vol. 15, no. 1, pp. 1-11, 2025. [CrossRef] [Google Scholar] [Publisher Link]

[34] Md. Masud Rana, Md. Ariful Islam, and Ibrahim M. Mehedim "Dual-Band Implantable Antenna Loaded with Patch Slots for Wireless Biotelemetry Systems," *Progress in Electromagnetics Research C*, vol. 141, pp. 151-162, 2024. [CrossRef] [Google Scholar] [Publisher Link]

[35] Jamel Smida et al., "A Compact Implantable Multiple-Input-Multiple-Output Antenna for Biotelemetry and Sensing Applications," *Sensors*, vol. 25, no. 11, pp. 1-18, 2025. [CrossRef] [Google Scholar] [Publisher Link]

[36] Zongsheng Gan et al., "A Small Implantable Compact Antenna for Wireless Telemetry Applied to Wireless Body Area Networks," *Applied Sciences*, vol. 15, no. 3, pp. 1-18, 2025. [CrossRef] [Google Scholar] [Publisher Link]